



Article

Microstrip Quasi-Elliptic Absorptive Bandpass Filter with Ultra-Wide Reflectionless Range and Compact Size

Awei Zhang ^{1,*}, Jinping Xu ¹, Zhiqiang Liu ² and Yuwei Zhang ¹

¹ State Key Laboratory of Millimeter Waves, Southeast University, Nanjing 210096, China; jpxu@seu.edu.cn (J.X.); yuwei_zzz@163.com (Y.Z.)

² Pervasive Communication Research Center, Purple Mountain Laboratories, Nanjing 211111, China; seulzq@163.com

* Correspondence: a_wei_zhang@seu.edu.cn

Abstract: Absorptive bandpass filters (ABPFs) are highly attractive in modern microwave communication systems due to their ability to internally absorb the harmful stopband RF-power reflections. This paper reports an approach to designing quasi-elliptic ABPFs with ultra-wide reflectionless range, enhanced selectivity, and compact size. The method is realized based on a fourth-order quasi-elliptic absorptive lowpass filter (ALPF) prototype with a simplified structure. This ALPF prototype exhibits both good impedance-matching over the whole normalized frequency domain and an adjustable transmission zero close to the passband. By applying an equivalent impedance transformer model, a coupled-line-based ABPF scheme is devised from the ALPF prototype, which eliminates conventional dispersive transmission line inverters, resulting in an ultra-wide reflectionless range and a compact size. Closed-form equations are derived to support the filter synthesis. A 2.45 GHz microstrip ABPF with 30% fractional bandwidth is designed for verification. The measured minimum in-band insertion loss is 0.83 dB and the reflectionless range of return loss better than 10 dB is from DC to 12.88 GHz. Both the upper and lower stopband suppression exceed 20 dB, with the upper stopband extending up to 6.80 GHz. The upper and lower out-of-band roll-off rates are 93.9 and 121.4 dB/GHz, respectively. The overall circuit size is $0.12 \lambda_g^2$.

Keywords: bandpass filter; absorptive filter; quasi-elliptic filter; transmission zero; reflectionless range



Citation: Zhang, A.; Xu, J.; Liu, Z.; Zhang, Y. Microstrip Quasi-Elliptic Absorptive Bandpass Filter with Ultra-Wide Reflectionless Range and Compact Size. *Electronics* **2024**, *13*, 1841. <https://doi.org/10.3390/electronics13101841>

Academic Editor: Giorgio Vannini

Received: 22 April 2024

Revised: 5 May 2024

Accepted: 7 May 2024

Published: 9 May 2024



Copyright: © 2024 by the authors. Licensee MDPI, Basel, Switzerland. This article is an open access article distributed under the terms and conditions of the Creative Commons Attribution (CC BY) license (<https://creativecommons.org/licenses/by/4.0/>).

1. Introduction

Elliptic/quasi-elliptic bandpass filters (BPFs) have been widely used in modern wireless communication systems due to their sharp out-of-band roll-off performance [1,2]. Nevertheless, these conventional BPFs suffer from the shortcoming that the RF signals within the stopband are reflected into the adjacent active components, which probably causes undesired intermodulation production in the mixer and sharp gain fluctuations in the amplifier, thus degrading the performance of RF front-end circuits [3,4]. To address this issue, increasing attention has been paid to developing absorptive/reflectionless filters that can internally dissipate reflection energy [5].

So far, absorptive bandpass filters (ABPFs) based on a variety of approaches and topologies have been reported in the literature. In refs. [6,7], a symmetrical circuit topology with even- and odd-mode subnetworks complementary to each other is proposed to implement ABPFs with lumped elements and transmission lines. By exploiting a back-to-back divider/coupler-based balanced circuit, a series of absorptive frequency-tunable BPFs or single/dual-passband ABPFs with symmetrical reflectionless behavior are presented in [8,9]. In refs. [10–18], a complementary-duplexer architecture is utilized to implement single/dual-port absorptive single/dual-band BPFs and frequency-adaptive BPFs. The work in [19–21] proposes an absorptive lowpass filter prototype (ALPF) to

realize ABPFs with a more concise structure. Nevertheless, most of the ABPFs mentioned above exhibit Butterworth or Chebyshev responses, which cannot satisfy the increasingly stringent demands for suppressing adjacent channel interference in modern wireless communication systems.

For achieving enhanced selectivity, absorptive quasi-elliptic BPFs have been proposed, as reported in [22–26]. In ref. [22], a third-order tunable ABPF with a quasi-elliptic transmission response is proposed based on the image parameter method, but the extraction of element value and the implementation procedure are complicated. In ref. [23], based on the complementary duplexer architecture, high-order input-reflectionless microstrip BPFs using double-transmission-zero-generation cells in the bandpass filtering channel to achieve a quasi-elliptic response are presented. By using a power divider and a power combiner to form a balanced-circuit reflectionless filter, combined with the transverse signal interference technique to generate transmission zeros, a quasi-elliptic ABPF is designed in [24], but the circuit structure is complex. In refs. [25,26], a multilayered duplexer-based structure combined with microstrip-to-microstrip vertical transitions and slot-line resonators is exploited to develop wideband quasi-elliptic ABPFs. However, the multilayered structure results in extra difficulties in manufacturing and integration. Furthermore, one common disadvantage of these quasi-elliptic ABPFs [22–26] is that their circuit size is almost twice or more that of traditional reflective-type filters due to the adoption of multistage inverters [22,23], additional power dividers [24] and complex multilayered structures [25,26], which violates the miniaturization requirements of modern wireless communication systems. On the other hand, most of the distributed-element ABPFs mentioned above suffer from a restricted reflectionless range in practice, typically between $0.5 f_0$ and $2.5 f_0$ (f_0 : center frequency) [8,9,12–24,26], caused by the limited bandwidth of the couplers/power-dividers or the dispersion of transmission-line inverters, which is also an important issue that needs to be addressed urgently.

In this paper, an approach to designing quasi-elliptic ABPFs with an ultra-wide reflectionless range and compact size is presented. This method is implemented based on a fourth-order quasi-elliptic ALPF prototype that is structurally simplified compared to the classical duplexer architecture [13,23]. This ALPF prototype exhibits not only good impedance matching in the passband and stopband but also a flexible transmission zero near the passband. By means of rigorous circuit transformations and an equivalent impedance transformer model, a coupled-line-based ABPF scheme eliminating dispersive transmission line inverters is derived from the ALPF prototype, which leads to the feasibility of realizing an ultra-wide reflectionless range and a compact size. A 2.45 GHz microstrip quasi-elliptic ABPF with 30% fractional bandwidth is designed and tested for verification. The measured results show reasonable agreement with the simulated ones, which validates the design concept.

2. Design Procedure for the Quasi-Elliptic ABPF

2.1. Schematic and Analysis of the Quasi-Elliptic ALPF Prototype

The schematic of the proposed fourth-order quasi-elliptic ALPF prototype with a simplified ladder network structure is illustrated in Figure 1a, which is constructed by adding an absorptive (matching) section at the input port of a traditional reflective-type elliptic LPF prototype. The absorptive section, composed of a resistor g_R and a capacitor $g_{C,1}$ in series, is connected in parallel in the ladder network and applied to dissipate the reflected signal of the stopband (match impedance). The lossless reactance elements $g_{L,1}$, $g_{L,2}$, $g_{C,2}$, $g_{L,3}$, $g_{L,4}$ and $g_{C,3}$, following the absorptive section, are arranged according to the topology of the conventional reflection-type elliptic LPF prototype. The reflection coefficient of the proposed quasi-elliptic ALPF at the input port can be expressed as follows:

$$S_{11} = \frac{Z_a \cdot Z_b - (Z_a + Z_b)}{Z_a \cdot Z_b + Z_a + Z_b} \quad (1)$$

where

$$Z_a = g_R + \frac{1}{sg_{C,1}}, \quad Z_b = sg_{L,1} + \frac{1}{\frac{1}{sg_{L,2} + \frac{1}{sg_{C,2}}} + \frac{1}{sg_{L,3} + \frac{1}{sg_{C,3} + 1}}}. \quad (2)$$

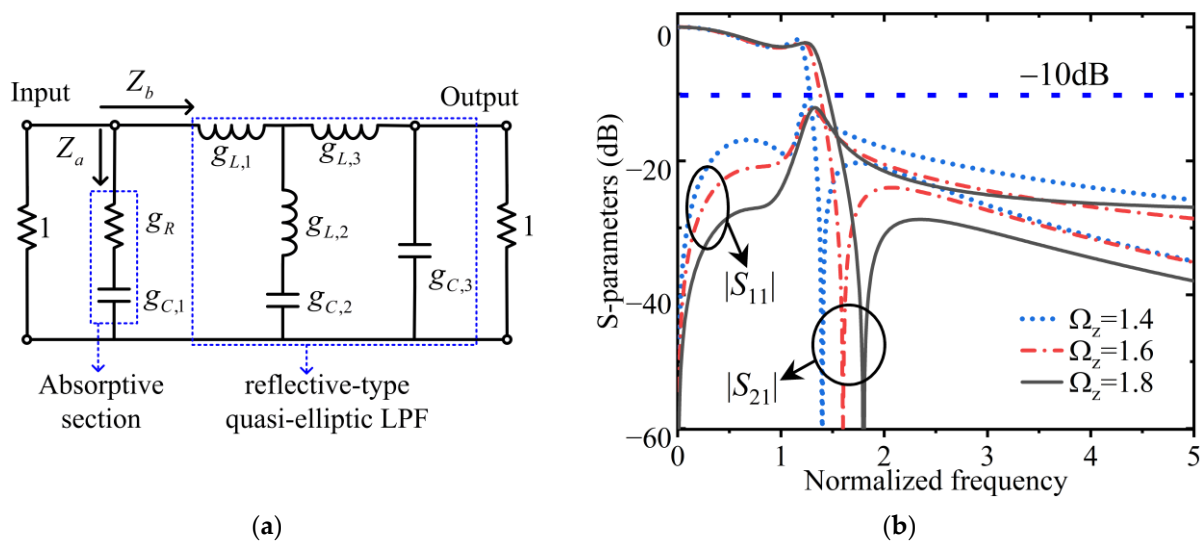


Figure 1. Schematic and frequency responses of the proposed 4th-order quasi-elliptic ALPF prototype. (a) Schematic; (b) frequency responses of the ALPF prototype adopting the parameter values in Table 1.

Table 1. Parameter values of normalized lumped elements.

Ω_Z	g_R	$g_{C,1}$	$g_{L,1}$	$g_{L,2}$	$g_{C,2}$	$g_{L,3}$	$g_{C,3}$
1.4	1.0	0.886	1.277	1.473	0.346	1.277	0.470
1.6	1.0	0.982	1.207	0.839	0.464	1.207	0.513
1.8	1.0	1.011	1.164	0.540	0.571	1.164	0.608

It turns out from (1) and (2) that the reflectionless behavior ($S_{11} = 0$) at the input port can be obtained when $Z_a \cdot Z_b = Z_a + Z_b$ is satisfied. Meanwhile, the proposed ALPF possesses an adjustable transmission zero (TZ) at finite frequencies of Ω_Z in the transmission response, where

$$\Omega_Z = \frac{1}{\sqrt{g_{L,2} \cdot g_{C,2}}} \quad (3)$$

By properly configuring the g-parameter values of the ALPF prototype, not only a low reflection response in the passband and stopband but also a high-selectivity transmission response with a TZ close to the passband can be achieved.

The S-parameter matrix of the proposed quasi-elliptic ALPF can be expressed as

$$S = \begin{bmatrix} S_{11} & S_{12} \\ S_{21} & S_{22} \end{bmatrix} \quad (4)$$

The following constraint conditions are prescribed to obtain the g-parameters, as was applied in [21]:

$$\begin{aligned} |S_{11}(\Omega)|^2 &\leq 10^{-RL/10} \\ |S_{21}(\Omega=0)|^2 &= 1 \\ |S_{21}(\Omega=1)|^2 &= 0.5 \\ |S_{21}(\Omega=\Omega_Z)|^2 &= 0 \end{aligned} \quad (5)$$

where RL is the predefined minimum return loss. With the above constraint conditions, three sets of g -parameter values are obtained to produce the pre-specified responses with TZ at $\Omega_Z = 1.4$, $\Omega_Z = 1.6$ and $\Omega_Z = 1.8$, respectively. The procedure of obtaining these three sets of g -parameter values is facilitated by utilizing the Nominal Optimization function of the EM simulation software Advanced Design System (ADS) 2015.01 with a random optimizer and a gradient optimizer. The derived g -parameter values are given in Table 1, where $RL = 10$ dB and $g_{L,1} = g_{L,3}$ is adopted. Figure 1b depicts the frequency responses of the ALPF adopting the g -parameter values in Table 1. It is observed that three sets of responses with different TZs satisfy the restraints specified by (5), that is, the insertion losses are 3 dB at the cutoff frequency of $\Omega = 1$ and the return losses are better than 10 dB over all normalized frequencies.

2.2. Lowpass to Bandpass Transformation

With lowpass to bandpass transformation [27], the capacitors and inductors in Figure 1a are transformed into parallel and series LC resonators, respectively. Then, impedance scaling and Richard's Transformation are applied to obtain the distributed-element quasi-elliptic ABPF circuit using quarter-wavelength stubs [27], as illustrated in Figure 2.

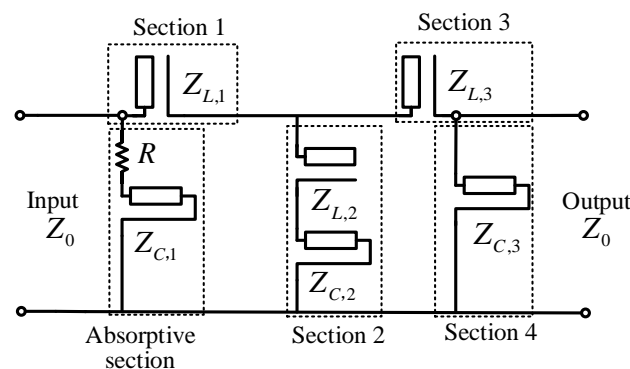


Figure 2. Schematic of the 4th-order quasi-elliptic ABPF using quarter-wavelength stubs.

The impedances at the input and output ports are set to Z_0 . A quarter-wavelength open circuit stub in series is equivalent to an LC series resonator and a quarter-wavelength short circuit stub is equivalent to an LC parallel resonator. Their characteristic impedance can be expressed as [27]

$$Z_{L,i} = \frac{Z_0 4g_{L,i}}{FBW \cdot \pi}, \quad Z_{C,i} = \frac{Z_0 FBW \cdot \pi}{4g_{C,i}} \quad (i = 1 \text{ to } 3), \quad (6)$$

where $g_{L,i}$ is the value of the normalized inductor, $g_{C,i}$ denotes the value of the normalized capacitor and FBW represents the desired fractional bandwidth. After impedance scaling, the resistance of the loaded resistor in the absorptive section can be obtained and expressed as [27]

$$R = Z_0 \cdot g_R. \quad (7)$$

According to Equation (6), the bandwidth of the ABPF can be adjusted by varying the characteristic impedance value of the open and short circuit stubs. Figure 3a demonstrates the frequency responses of the quasi-elliptic ABPF with a pair of TZs at $\Omega_Z = \pm 1.4$ under different fractional bandwidths (FBWs). It can be observed that the quasi-elliptic ABPF exhibits a good return loss both in the passband and stopband under different FBWs.

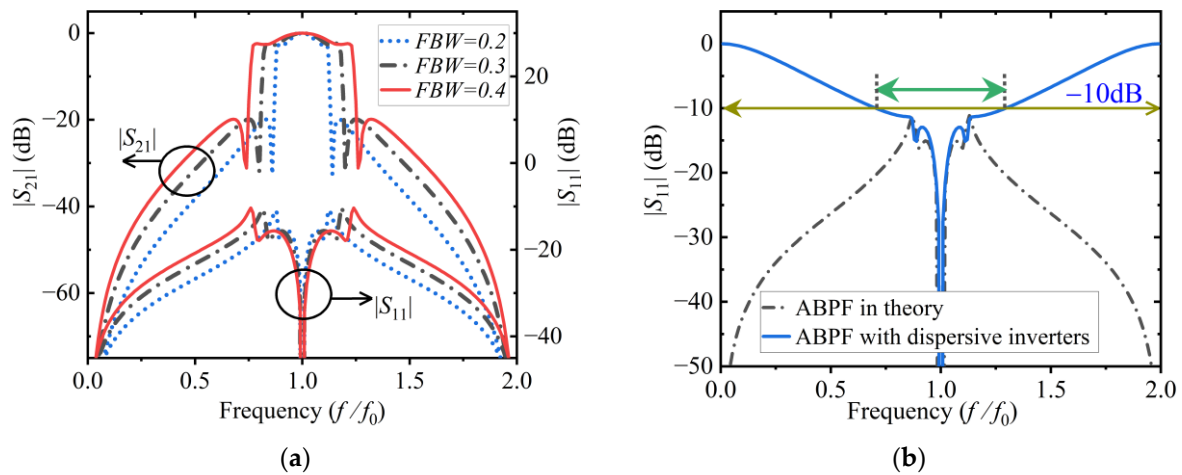


Figure 3. Frequency response of the quasi-elliptic ABPF. (a) Frequency response of the quasi-elliptic ABPF under different FBWs; (b) effect of the dispersive inverter on the reflectionless response.

2.3. Equivalent Impedance Transformer Circuit Model

The quasi-elliptic ABPF circuit using quarter-wavelength stubs shown in Figure 2 is difficult to implement in practice due to its series and parallel branches containing series open circuit stubs. In conventional methods, transmission-line inverters are generally applied to convert series open circuit stubs into realizable parallel short circuit stubs, as presented in [13,14,16,18–20,22,23]. However, the actual transmission-line inverters exhibit frequency-variant (dispersive) characteristics, which deteriorate the reflectionless performance of the distributed-element ABPF. As illustrated in Figure 3b, the reflectionless range ($|S_{11}| \leq -10$ dB) of the ABPF using dispersive transmission-line inverters is substantially reduced compared to the theoretical value. Furthermore, the adoption of multistage quarter-wavelength transmission-line inverters also leads to a significant increase in the overall circuit size.

This work aims to find an equivalent circuit to the distributed-element ABPF circuit shown in Figure 2 to make it implementable and to eliminate the restriction to reflectionless bandwidth caused by conventional dispersive transmission-line inverters. To this end, an equivalent impedance transformer model is introduced to convert the series open circuit stubs into realizable coupled line units. As illustrated in Figure 4a, the three-port coupled line network on the left side has the same network parameters as the three-port network with the impedance transformer on the right side, provided the following Equations (8) and (9) are satisfied, according to the relevant analyses in [28]:

$$Z_{\text{even}} = Z_A(1 + 1/n), \quad Z_{\text{odd}} = Z_A(1 - 1/n), \quad (8)$$

$$n = \sqrt{Z_B/Z_A + 1}, \quad (9)$$

where Z_{even} and Z_{odd} are the modal impedances of the coupled lines, Z_A denotes the characteristic impedance of the series transmission line and Z_B represents the characteristic impedance of the parallel open circuit stubs. All lines have the same electrical length of $\pi/4$. It should be noted that the introduction of the equivalent impedance transformer model brings about impedance ratios of $n:1$ that should be kept the same at the same node in the network to prevent the mismatching of impedances.

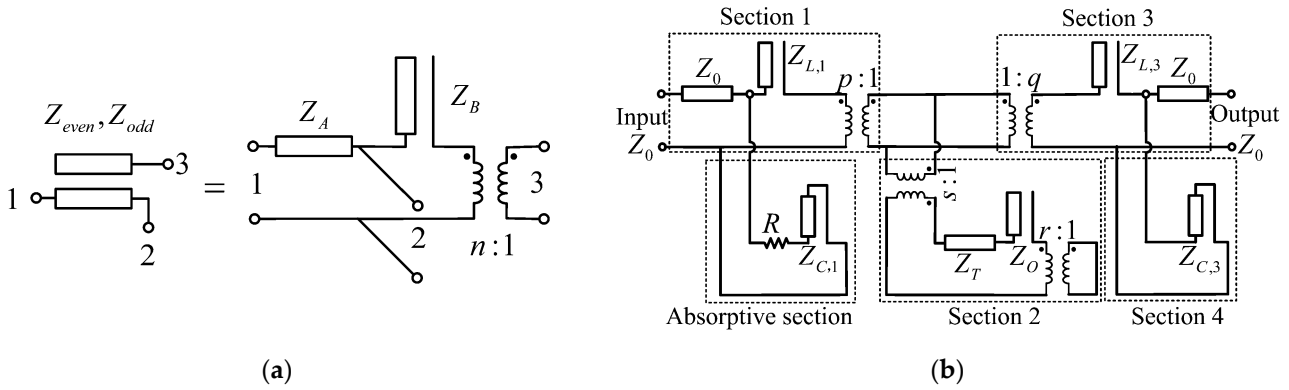


Figure 4. The equivalent impedance transformer circuit model. (a) Equivalent impedance transformer circuit model of the coupled line; (b) equivalent circuit of the ABPF circuit in Figure 2.

Based on the analysis above, an equivalent impedance transformer model of the ABPF circuit in Figure 2 is derived, as shown in Figure 4b. Firstly, two transmission lines with a characteristic impedance of Z_0 are inserted at the input and output ports to match the source and load without altering the frequency response of the filter. Secondly, the positions of the quarter-wavelength transmission line and open circuit stub in Section 2 are exchanged using Kuroda's identity without changing the input impedance of the overall parallel section [29]. Then, the impedances of the quarter-wavelength transmission line and the open circuit stub are transformed into

$$Z_T = Z_{L,2} + Z_{C,2}, \quad Z_O = (Z_{L,2} + Z_{C,2})Z_{L,2}/Z_{C,2}. \quad (10)$$

At last, two transformers with ratios of $p:1$ and $1:q$ are introduced in Sections 1 and 3, and two transformers with ratios of $s:1$ and $r:1$ are introduced at two ends of Section 2, for transforming each section containing the open circuit stubs in series into practically realizable coupled lines. The parallel short circuit stubs in the absorptive section and Section 4 remain unchanged.

2.4. Coupled-Line-Based Quasi-Elliptic ABPF Scheme

Based on the equivalent impedance transformer model in Figure 4b, a coupled-line-based quasi-elliptic ABPF scheme is devised that avoids the adoption of dispersive transmission line inverters, as illustrated in Figure 5.

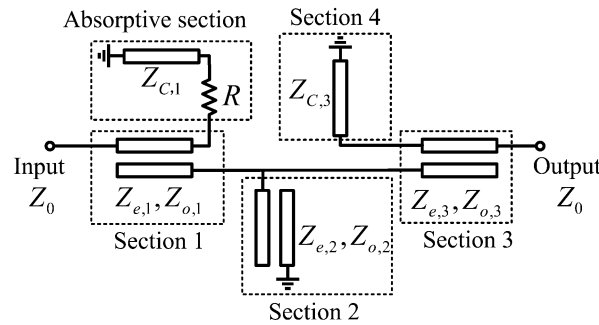


Figure 5. Schematic of the quasi-elliptic ABPF based on coupled line units.

The modal impedances of the coupled line units in Sections 1–3 of the ABPF circuit are expressed as

$$Z_{e,1} = Z_0(1 + 1/p), \quad Z_{o,1} = Z_0(1 - 1/p), \quad (11)$$

$$Z_{e,2} = (1 + 1/r)Z_T/s^2, \quad Z_{o,2} = (1 - 1/r)Z_T/s^2, \quad (12)$$

$$Z_{e,3} = Z_0(1 + 1/q), Z_{o,3} = Z_0(1 - 1/q). \quad (13)$$

The ABPF circuit using coupled line units shown in Figure 5 possesses the same frequency response as that of the ideal distributed circuit shown in Figure 2, provided that the following, Equations (14) and (15), are satisfied:

$$p = q = s = \sqrt{Z_{L,1}/Z_0 + 1} = \sqrt{Z_{L,3}/Z_0 + 1}. \quad (14)$$

$$r = \sqrt{Z_O/Z_T + 1}. \quad (15)$$

Equation (14) requires that the parameter value of $g_{L,1}$ be equal to $g_{L,3}$. In summary, based on the parameter values in Table 1 and Equations (6)–(15), a coupled-line-based quasi-elliptic ABPF can be fulfilled, which not only eliminates the restriction to reflectionless bandwidth caused by conventional dispersive transmission-line inverters but also achieves a compact size.

Considering the fabrication accuracy of the printed circuit board (PCB) process, there is a limitation on the proposed ABPF in terms of the achievable passband bandwidth due to the adoption of a coupled line structure. The coupling coefficient of the coupled line unit is defined as [27]

$$C = \frac{Z_e - Z_o}{Z_e + Z_o}, \quad (16)$$

where Z_e and Z_o are the even-mode impedance and odd-mode impedance of the coupled line, respectively. According to Equations (6) and (10)–(16), the coupling coefficient of the coupled line increases and the required coupled gap spacing decreases when the filter FBW increases. For the proposed quasi-elliptic ABPF shown in Figure 5, the coupling coefficient of the coupled line unit in Section 1 is equal to that of the coupled line unit in Section 3 and larger than that of the coupled line unit in Section 2. Therefore, the minimum spacing that can be implemented for the coupled line in Section 1 determines the maximum achievable bandwidth of the proposed ABPF. For example, to achieve a quasi-elliptic ABPF with an FBW of 40%, the gap spacing of the coupled lines is required to be less than 0.05 mm if a common single-layer substrate (for example, an RO4350B substrate with a dielectric constant of 3.66 and a thickness of 0.508 mm) is adopted. However, the 0.05 mm gap spacing for the coupled line structure is very challenging to realize with the conventional PCB process. Therefore, it is recommended to limit the FBW of the designed quasi-elliptic ABPF to no more than 35% to meet the requirements for machining accuracy of the PCB process.

3. Implementation and Discussion

3.1. Simulation and Measurement Results

To verify the proposed design concept, a microstrip quasi-elliptic ABPF, centered at 2.45 GHz, with an FBW of 30% was designed, fabricated and measured. The parameter values for the ALPF prototype in the first row of Table 1 were adopted. According to design Equations (6)–(15), the characteristic impedances of the short circuit stubs in the absorptive section and Section 4 were calculated as $Z_{C,1} = 13.3 \Omega$ and $Z_{C,3} = 25.1 \Omega$; the modal impedances of the coupled lines in Section 1 to Section 3 were calculated as $Z_{e,1} = 69.7 \Omega$, $Z_{o,1} = 30.3 \Omega$, $Z_{e,2} = 70.9 \Omega$, $Z_{o,2} = 37.1 \Omega$, $Z_{e,3} = 69.7 \Omega$ and $Z_{o,3} = 30.3 \Omega$. The resistance of the lumped resistor was 50 Ω . Based on the above design parameters, the initial physical dimensions of the microstrip quasi-elliptic ABPF could be obtained. The electromagnetic simulation software ANSYS High Frequency Structural Simulator (HFSS) 2021 R1 was used for optimization, utilizing its parameter sweep function and sequential nonlinear programming optimizer. In order to obtain accurate simulation results, the embedded effects of the SMA connectors were taken into account in the simulation process. Figure 6a presents the configuration of the quasi-elliptic ABPF prototype. The

optimized physical dimensions are given in Table 2. Adopting these physical dimensions, the designed quasi-elliptic ABPF with a compact circuit size of $0.12 \lambda_g^2$ was fabricated. The Rogers RO4350B substrate with a thickness of 0.508 mm ($\epsilon_r = 3.66$, $\tan\delta = 0.004$) was adopted in the fabrication. The photograph of the fabricated ABPF prototype is illustrated in Figure 6b.

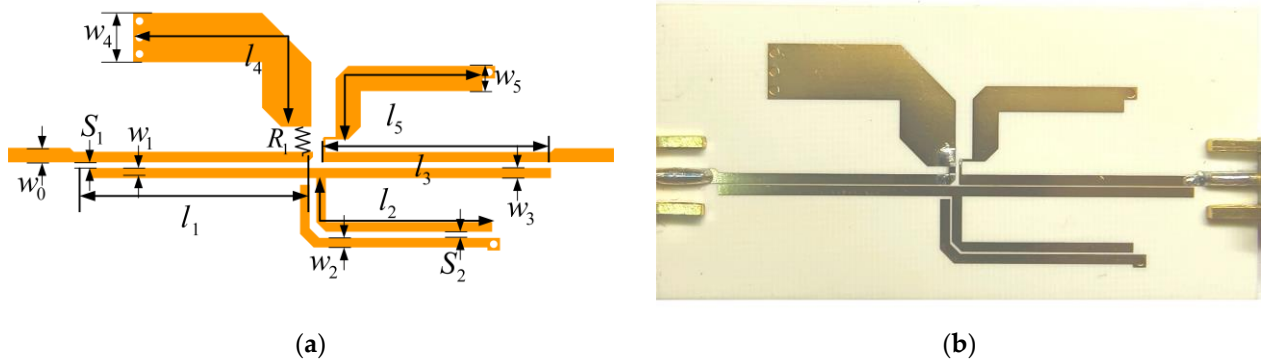


Figure 6. The configuration and photograph of the proposed quasi-elliptic ABPF. (a) Configuration; (b) photograph.

Table 2. Optimized physical dimensions of the designed ABPF. Unit: mm.

w_0	w_1	w_2	w_3	w_4	w_5	l_1
1.10	0.80	0.76	0.80	4.30	2.00	18.2
l_2	l_3	l_4	l_5	S_1	S_2	R_1
16.7	18.1	19.6	17.5	0.10	0.15	51.0

The fabricated ABPF prototype was measured using an Agilent E8363C vector network analyzer. Figure 7 shows the measured and simulated S-parameters. Within the pre-specified passband range of 2.08 GHz to 2.82 GHz, the minimum and maximum in-band insertion losses were 0.83 dB and 3.89 dB, respectively. The measured 3 dB passband was from 2.09 GHz to 2.81 GHz. The return loss was better than 10 dB from DC to 12.88 GHz, which is commonly viewed as the reflectionless range. Two TZs near the passband were located at 1.99 GHz and 3.01 GHz. Both the upper and lower stopband suppression were larger than 20 dB, and the upper stopband was up to 6.80 GHz. The upper and lower out-of-band roll-off rates were 93.9 dBc/GHz and 121.4 dBc/GHz (attenuation: 20 dB at 2.0 GHz and 2.94 GHz), respectively. It can be observed that the measured passband bandwidth was slightly smaller than the simulated one. The main reason for this difference is that the gap spacing S_2 between the coupled lines of the fabricated filter prototype is slightly larger than the design value, which is caused by the limitation of PCB processing accuracy. In addition to the S-parameter, the measured group delay is also illustrated in Figure 8. Within the 3 dB passband, the measured minimum and maximum group delay values were 1.12 ns and 1.38 ns, respectively, which indicate a good phase response.

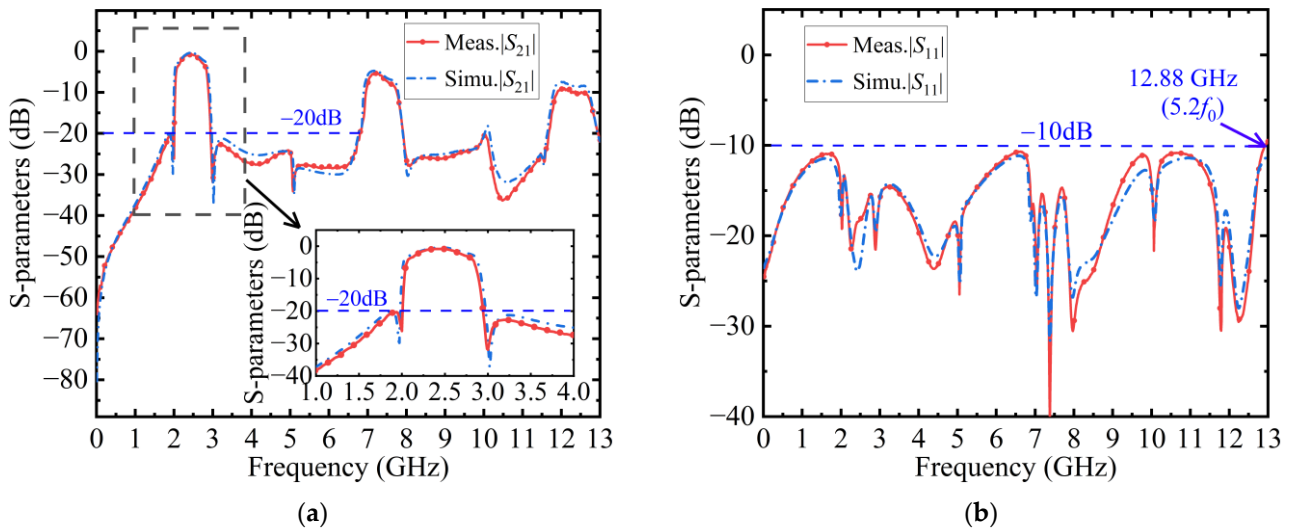


Figure 7. Simulated and measured S-parameter of the proposed ABPF. (a) S_{21} ; (b) S_{11} .

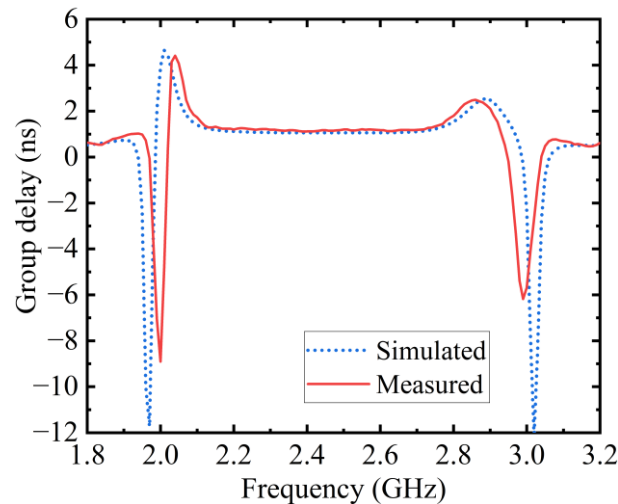


Figure 8. Simulated and measured group delay of the proposed ABPF.

3.2. Discussion and Recommendation

It can be observed from Figures 7 and 8 that the simulated and measured frequency responses are in reasonable agreement with each other, which verifies the feasibility and validity of the proposed method for designing microstrip quasi-elliptic ABPFs. The performance compared with other state-of-the-art works [8,14–17,23,24,26] is shown in Table 3. Compared with the ABPFs described in [8,14–17], the proposed ABPF features a higher upper/lower out-of-band roll-off rate due to having two transmission zeros close the passband. The absorptive BPF proposed in [23] exhibits a quasi-elliptic-type transmission response and a wide stopband; however, the reflectionless range is restricted due to the adoption of multistage quarter-wavelength dispersive inverters. As a comparison, the reflectionless range of the proposed quasi-elliptic ABPF reaches up to $5.2f_0$ (f_0 is the center frequency of the passband), which is a significant advancement over the presented ABPFs in [8,14–17,23,24,26]. The quasi-elliptic ABPF reported in [24] has a complex structure due to containing multiple filter channels and additional circuits, resulting in a relatively larger circuit size. In ref. [25], a multilayered structure with microstrip-to-microstrip vertical transitions is applied to realize quasi-elliptic ABPFs with a wide reflectionless range, while the multilayered structure also brings extra difficulties in manufacturing and integration, suffering from the same shortcoming of uncompact circuit size as the ABPF in [23,24]. In

comparison, another key attribute of the proposed ABPF is its simple structure and compact size, which have advantages in modern microwave wireless communication systems with a tendency towards miniaturization. As can be seen from the comparison, the main advantage of the proposed quasi-elliptic ABPF that sets itself apart from the existing ABPFs and contributes to its novelty is the simultaneous realization of the ultra-wide reflectionless range, sharp roll-off and compact size.

Table 3. Comparison with the state-of-the-art works.

Ref.	f_0 (GHz)	IL (dB)	QET	Closed- Method	Order	Rejection /Stopband	U/L Roll-Off Rate (dBc/GHz)	Reflectionless Range	Size (λ_g^2)
[8]	2.00	1.40	No	No	2	30 dB/1.75 f_0	NA	0.7–1.3 f_0	0.22
[14]	2.49	0.90	No	Yes	2	20 dB/1.40 f_0	NA	0.6–1.3 f_0	0.78
[15]	2.45	1.10	No	No	3	NA	70.1/77.3 *	0.4–2.7 f_0	0.82
[16]	1.98	0.71	No	No	3	NA	39.5/43.5 *	0.2–1.8 f_0	0.39
[17]	2.03	0.52	No	Yes	4	NA	25.8/22.1 *	DC–2.2 f_0	0.66
[23]	1.96	0.95	Yes	Yes	3	20 dB/2.73 f_0	NA	0.5–1.5 f_0	1.09
[24]	2.98	2.20	Yes	Yes	2	30 dB/1.91 f_0	74.8/58.7	0.5–1.3 f_0	NA
[26]	1.98	0.75	Yes	Yes	6	28 dB/2.42 f_0	68.5/100.5 *	DC–2.8 f_0	1.97
This work	2.45	0.83	Yes	Yes	4	20 dB/2.77 f_0	93.9/121.4	DC–5.2 f_0	0.12

IL: minimum in-band insertion loss; QET: quasi-elliptic-type; reflectionless range: ($|S_{11}| \leq -10$ dB); U/L: upper/lower out-of-band; roll-off rate: $[20\text{dB} - 3\text{dB}] / |f_{-20\text{dB}} - f_{-3\text{dB}}|$; *: estimated from the results; NA: not available.

However, there is a limitation on the proposed coupled-line-based quasi-elliptic ABPF in terms of the achievable passband bandwidth, considering the fabrication accuracy of the printed circuit board (PCB) process. In order to further improve the bandwidth of the proposed quasi-elliptic ABPF, an efficient solution is to substitute the conventional coupled microstrip lines used in this design with the broadside coupled transmission lines with higher coupling coefficients presented in [30].

It is worth noting that the proposed quasi-elliptic ABPF has a relatively large insertion loss at the passband edges, resulting in an in-band amplitude flatness of about 3 dB, as illustrated in Figure 7a. An explanation for this is that the first-order absorptive section and the fourth-order conventional reflection-type filter are not perfectly matched at the transition band, resulting in part of the energy being consumed by the absorptive section. To further reduce the insertion loss at the passband edges as well as the in-band amplitude flatness, an effective method is to use a higher-order absorptive section for better impedance matching at the transition band. But further studies may be required to make the higher-order absorptive section implementable and not affect the reflectionless range of the filter. Additionally, if we want to further improve the overall insertion loss in the passband, the suspended coplanar waveguide with lower dielectric loss can be used to replace the microstrip line in this design, as applied in [31].

In order to increase the utility of the proposed quasi-elliptic ABPF in demanding RF environments, the performance of the filter in rejecting out-of-band signals can be further improved. To this end, an effective method is to increase the order of the filter to introduce additional transmission zeros (TZs). For example, a high-order quasi-elliptic ALPF prototype is illustrated in Figure 9a, which has two series resonators in the parallel branches of Section 2 and Section 4 in the filter network. These two series resonators introduce two controllable TZs in the filter transmission response at finite frequencies of $\Omega_{Z1} = 1/\sqrt{g_{L,2} \cdot g_{C,2}}$ and $\Omega_{Z2} = 1/\sqrt{g_{L,4} \cdot g_{C,3}}$, respectively. By utilizing the combinations of these two TZs, the out-of-band rejection levels of the proposed quasi-elliptic filter can be further enhanced.

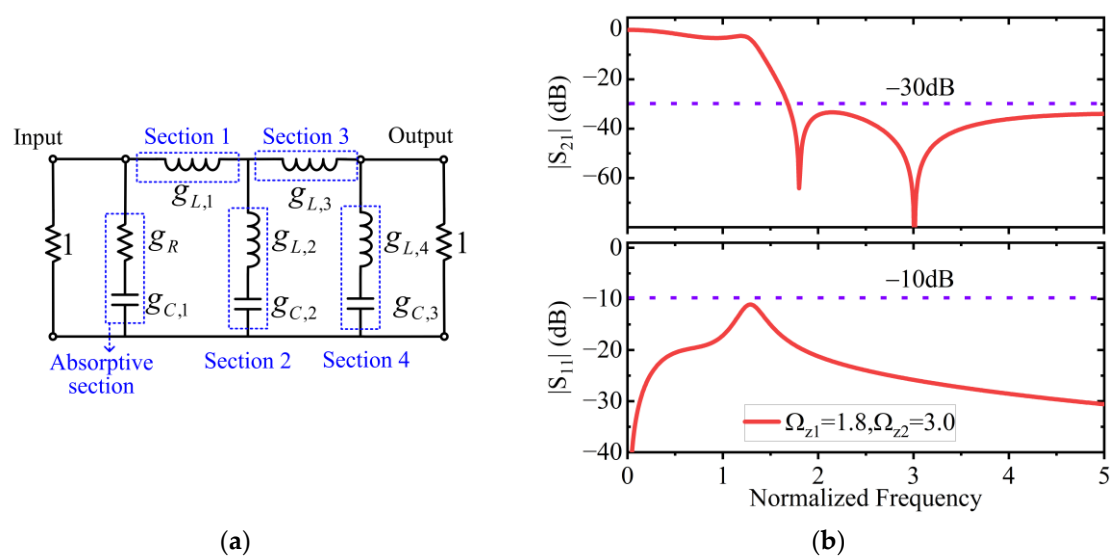


Figure 9. Schematic and frequency responses of a high-order quasi-elliptic ALPF prototype with two TZs. (a) Schematic; (b) frequency responses.

Figure 9b illustrates the transmission response of the high-order ALPF prototype shown in Figure 9a. As can be seen, through a combination of the two TZs at $\Omega_Z = 1.8$ and $\Omega_Z = 3.0$, an out-of-band rejection level higher than 30 dB is achieved. At the same time, a low reflection response with return losses of better than 10 dB is also realized over all normalized frequencies. In accordance with the design methodology proposed in this paper, a high-order coupled-line-based quasi-elliptic ABPF with two pairs of TZs can be designed based on the ALPF prototype shown in Figure 9a.

4. Conclusions

In this paper, a method for designing compact microstrip ABPFs with enhanced selectivity and an ultra-wide reflectionless range is reported. Based on the proposed quasi-elliptic ALPF prototype with a set of given g-parameters and rigorous circuit transformations, the design procedure for a couple-line-based quasi-elliptic ABPF is detailed. The design equations supporting the filter synthesis are derived. A 2.45 GHz microstrip ABPF is designed, fabricated and tested. The measured 3 dB passband is from 2.09 GHz to 2.81 GHz, with a reflectionless range of DC to 12.88 GHz. The measured minimum in-band insertion loss is 0.83 dB. Both the upper and lower stopband suppression are larger than 20 dB, and the upper stopband extends up to 6.80 GHz. The upper and lower out-of-band roll-off rates are 93.9 dB/GHz and 121.4 dB/GHz, respectively. The measured results validate the feasibility of the proposed design method. The devised ABPF exhibits a simple structure, a high-selectivity transmission response, an ultra-wide reflectionless range and a compact size, which has good application potential in 5G/6G advanced communication systems.

Author Contributions: Conceptualization, A.Z.; data curation, A.Z.; formal analysis, A.Z. and Z.L.; investigation, A.Z. and Y.Z.; methodology, A.Z.; software, A.Z.; validation, A.Z., Z.L. and Y.Z.; visualization, A.Z.; writing—original draft, A.Z. and J.X.; project administration, J.X.; funding acquisition, J.X.; resources, J.X.; supervision, J.X.; writing—review and editing, J.X. and Z.L. All authors have read and agreed to the published version of the manuscript.

Funding: This research was supported by the Natural Science Foundation of Jiangsu Province under Grant BK20230133.

Data Availability Statement: All data are included within the manuscript.

Conflicts of Interest: The authors declare no conflicts of interest regarding the publication of this article.

References

1. Yang, L.; Gómez-García, R. High-order quasi-elliptic-type single-ended and balanced wideband bandpass filters using microstrip-to-microstrip vertical transitions. *IEEE Trans. Circuits Syst. II Exp. Briefs* **2023**, *70*, 1425–1429. [\[CrossRef\]](#)
2. Chu, Q.-X.; Qiu, L.-L. Wideband balanced filters with high selectivity and common-mode suppression. *IEEE Trans. Microw. Theory Tech.* **2015**, *63*, 3462–3468. [\[CrossRef\]](#)
3. Li, X.; Xing, M.; Liu, G.; Yang, X.; Dai, C.; Hou, M. Compact, reflectionless band-pass filter: Based on GaAs IPD process for highly reliable communication. *Electronics* **2021**, *10*, 2998. [\[CrossRef\]](#)
4. Moon, S.-M.; Lee, H.L.; Lee, M.-Q. Absorptive K-band bandpass filter using a balanced recursive structure. *Electronics* **2020**, *9*, 1633. [\[CrossRef\]](#)
5. Zhang, S.; Liu, H.; Chen, S.; Wang, Z.; Fang, S. Synthesis of wideband all-frequency absorptive filtering power divider with high selectivity and flat output port distributions. *Electronics* **2023**, *12*, 3704. [\[CrossRef\]](#)
6. Morgan, M.A.; Boyd, T.A. Theoretical and experimental study of a new class of reflectionless filter. *IEEE Trans. Microw. Theory Tech.* **2011**, *59*, 1214–1221. [\[CrossRef\]](#)
7. Morgan, M.A.; Boyd, T.A. Reflectionless filter structures. *IEEE Trans. Microw. Theory Tech.* **2015**, *63*, 1263–1271. [\[CrossRef\]](#)
8. Lu, Q.-Y.; Wang, J.; Zhu, L.; Xia, Z.; Wu, W. Design of reflectionless bandpass filters based on asymmetric reciprocal filtering network. *IEEE Trans. Microw. Theory Tech.* **2023**; Early Access. [\[CrossRef\]](#)
9. Fan, M.; Song, K.; Yang, L.; Gomez-Garcia, R. Frequency-tunable constant-absolute-bandwidth single-/dual-passband filters and diplexers with all-port-reflectionless behavior. *IEEE Trans. Microw. Theory Tech.* **2021**, *69*, 1365–1377. [\[CrossRef\]](#)
10. Liu, C.; Deng, Z.; Liu, X.; Luo, X. A wideband bandpass filter with broad stopband and ultra-wide reflectionless range for 5G applications. In Proceedings of the 2019 IEEE MTT-S International Microwave Symposium (IMS), Boston, MA, USA, 2–7 June 2019; pp. 834–837. [\[CrossRef\]](#)
11. Lee, J.; Lee, J. Transmission-line bandpass filter structures with infinite reflectionless range. *IEEE Trans. Circuits Syst. I Reg. Pap.* **2022**, *69*, 2387–2398. [\[CrossRef\]](#)
12. Li, X.; Xiao, J. Reflectionless ultra-wideband bandpass filter based on suspended coplanar waveguide-microstrip broadside coupling. *AEU Int. J. Electron. Commun.* **2024**, *175*, 155100. [\[CrossRef\]](#)
13. Psychogiou, D.; Gómez-García, R. Reflectionless adaptive RF filters: Bandpass, bandstop, and cascade designs. *IEEE Trans. Microw. Theory Tech.* **2017**, *65*, 4593–4605. [\[CrossRef\]](#)
14. Gómez-García, R.; Muñoz-Ferreras, J.-M.; Psychogiou, D. Symmetrical quasi-absorptive RF bandpass filters. *IEEE Trans. Microw. Theory Tech.* **2019**, *67*, 1472–1482. [\[CrossRef\]](#)
15. Wu, X.; Li, Y.; Liu, X. High-order dual-port quasi-absorptive microstrip coupled-line bandpass filters. *IEEE Trans. Microw. Theory Tech.* **2020**, *68*, 1462–1475. [\[CrossRef\]](#)
16. Luo, C.; Wong, S.-W.; Lin, J.-Y.; Yang, Y.; Li, Y.; Yu, X.-Z.; Feng, L.-P.; Tu, Z.-H.; Zhu, L. Quasi-reflectionless microstrip bandpass filters using bandstop filter for out-of-band improvement. *IEEE Trans. Circuits Syst. II Exp. Briefs* **2020**, *67*, 1849–1853. [\[CrossRef\]](#)
17. Yang, L.; Gómez-García, R.; Muñoz-Ferreras, J.-M.; Zhang, R.; Peroulis, D.; Zhu, L. Multilayered reflectionless wideband bandpass filters with shunt/in-series resistively terminated microstrip lines. *IEEE Trans. Microw. Theory Tech.* **2020**, *68*, 877–893. [\[CrossRef\]](#)
18. Wei, F.; Xue, Y.-C.; Zhao, X.-B.; Liu, W.-S.; Xu, L.; Zhang, P.F. Balanced BPF with dual-port quasi-reflectionless characteristic and selectivity enhancement. *IEEE Trans. Circuits Syst. II Exp. Briefs* **2023**, *70*, 994–998. [\[CrossRef\]](#)
19. Jeong, S.-W.; Lee, T.-H.; Lee, J. Absorptive filter prototype and distributed-element absorptive bandpass filter. In Proceedings of the 2018 IEEE MTT-S International Conference on Numerical Electromagnetic and Multiphysics Modeling and Optimization (NEMO), Reykjavik, Iceland, 8–10 August 2018; pp. 1–4. [\[CrossRef\]](#)
20. Jeong, S.-W.; Lee, T.-H.; Lee, J. Frequency- and bandwidth-tunable absorptive bandpass filter. *IEEE Trans. Microw. Theory Tech.* **2019**, *67*, 2172–2180. [\[CrossRef\]](#)
21. Lee, T.-H.; Lee, B.; Kim, Y.-S.; Wu, K.; Lee, J. Higher order lumped element absorptive low-pass and bandpass filter structures. *IET Microw. Antennas Propag.* **2018**, *13*, 1166–1173. [\[CrossRef\]](#)
22. Cho, Y.H.; Park, C. Tunable Absorptive bandpass filter with two transmission zeros based on image parameter method. *IET Microw. Opt. Technol. Lett.* **2023**, *66*, 1. [\[CrossRef\]](#)
23. Gómez-García, R.; Muñoz-Ferreras, J.-M.; Psychogiou, D. High-order input-reflectionless bandpass/bandstop filters and multiplexers. *IEEE Trans. Microw. Theory Tech.* **2019**, *67*, 3683–3695. [\[CrossRef\]](#)
24. Malki, M.; Yang, L.; Gómez-García, R. Input-reflectionless quasi-elliptic-type single- and dual-band bandpass filters based on passive channelized principles. *IEEE Trans. Circuits Syst. I Reg. Pap.* **2023**, *70*, 190–202. [\[CrossRef\]](#)
25. Yang, L.; Zhu, X.; Gómez-García, R. High-order quasi-elliptic-type wideband bandpass filter with ultrabroad input-reflectionless stopband range. *IEEE Microw. Wirel. Technol. Lett.* **2023**, *33*, 655–658. [\[CrossRef\]](#)
26. Yang, L.; Gómez-García, R.; Fan, M.; Zhang, R. Multilayered input-reflectionless quasi-elliptic-type wideband bandpass filtering devices on diplexer-based structures. *IEEE Trans. Microw. Theory Tech.* **2022**, *70*, 122–138. [\[CrossRef\]](#)
27. Matthaei, G.L.; Young, L.; Jones, E.M.T. *Microwave Filters, Impedance-Matching Networks, and Coupling Structures*; Artech House: Dedham, MA, USA, 1980.
28. Nemoto, Y.; Kobayashi, K.; Sato, R. Graph transformations of non-uniform coupled transmission line networks and their application. *IEEE Trans. Microw. Theory Tech.* **1985**, *33*, 1257–1263. [\[CrossRef\]](#)

29. Lee, J.; Lee, J. Implementation of distributed-element foster section and its applications to bandpass filters. *IEEE Microw. Wireless Compon. Lett.* **2022**, *32*, 391–394. [[CrossRef](#)]
30. Tong, R.; Olsson, J.; Dancila, D. An improved analytical model for broadside coupled transmission line used on planar circuit. *AEU Int. J. Electron. Commun.* **2021**, *138*, 1434–8411. [[CrossRef](#)]
31. Xiao, J.; Zhang, J.; Pu, J. Analysis and implementation of self-packaged multi-layer suspended coplanar waveguide and its applications in filtering circuits. *IEEE Access* **2022**, *10*, 456–467. [[CrossRef](#)]

Disclaimer/Publisher’s Note: The statements, opinions and data contained in all publications are solely those of the individual author(s) and contributor(s) and not of MDPI and/or the editor(s). MDPI and/or the editor(s) disclaim responsibility for any injury to people or property resulting from any ideas, methods, instructions or products referred to in the content.